

Available online at www.sciencedirect.com

ScienceDirect

journal homepage: www.journals.elsevier.com/oceanologia

ORIGINAL RESEARCH ARTICLE

Investigation of tidal asymmetry in the Shatt Al-Arab river estuary, Northwest of Arabian Gulf

Ali Abdulridha Lafta*

Department of Marine Physics, Marine Science Center, University of Basrah, Iraq

Received 20 July 2021; accepted 21 January 2022

Available online xxx

KEYWORDSTidal asymmetry;
Harmonic analysis;
Tidal skewness;
Arabian Gulf;
Shatt Al-Arab river

Abstract Approximately one-year water level records were utilized for examining the tidal dynamics and tidal asymmetry at the Shatt Al-Arab river estuary. The harmonic and the tidal skewness, two traditional methods in quantifying tidal asymmetry in tidal systems, were used. The water level measurements revealed a presence of a tidal wave attenuation when propagating further towards the inland direction, with notable reductions in the tidal range. The results of the harmonic analysis indicated that the diurnal and semi-diurnal constituents experience considerable damping towards the upstream direction. The largest constituent was M2, followed by K1, O1, and S2. The largest shallow water constituent was MK3, followed by M4, MS4, MN4, and M6. The tidal form number ranged from 0.68 to 0.7 along the estuary; then, mixed, mainly semi-diurnal tidal nature was observed. However, six possible combinations of tidal constituents were used to quantify the tidal asymmetry, involving the interactions between astronomical constituents alone as well as with the higher harmonics. According to the harmonic method, the relative phase difference of M2 and M4 constituents was in the range of 63 to 87.06, suggesting a flood dominance behavior of tidal wave along the estuary. Positive values of the tidal skewness were observed at all stations, with a pronounced increase towards the inland direction. The M2 and M4 interaction was the main contributor to tidal asymmetry, followed by M2-K1-O1, M2-S2-MS4, M2-M4-M6, K1-M2-MK3, and M2-N2-MN4 interactions.

© 2022 Institute of Oceanology of the Polish Academy of Sciences. Production and hosting by Elsevier B.V. This is an open access article under the CC BY-NC-ND license (<http://creativecommons.org/licenses/by-nc-nd/4.0/>).

* Corresponding author at: Department of Marine Physics, Marine Science Center, University of Basrah, Iraq.

E-mail address: ali.lafta@uobasrah.edu.iq

Peer review under the responsibility of the Institute of Oceanology of the Polish Academy of Sciences.



<https://doi.org/10.1016/j.oceano.2022.01.005>

0078-3234/© 2022 Institute of Oceanology of the Polish Academy of Sciences. Production and hosting by Elsevier B.V. This is an open access article under the CC BY-NC-ND license (<http://creativecommons.org/licenses/by-nc-nd/4.0/>).

Please cite this article as: A.A. Lafta, Investigation of Tidal Asymmetry in the Shatt Al-Arab River Estuary, Northwest of Arabian Gulf, Oceanologia, <https://doi.org/10.1016/j.oceano.2022.01.005>

1. Introduction

The tidal wave generated in the ocean undergoes several changes when propagating towards the coastal regions, which are generally shallow water areas, leading to tidal wave asymmetry (Parker, 2007). The tidal asymmetry refers to the distortion of the tidal wave with an unequal duration of rising and falling tides, as well as the difference in the strength of the flood and ebb velocities (Friedrichs and Aubrey, 1988; Pugh, 1987). Tidal asymmetry plays a major role in sediment transport and water circulation in estuaries and coastal systems. The tide-averaged (residual) sediment movement in tidal environments is mainly related to its tidal asymmetry situation (Gatto et al., 2017; Hoitink et al., 2003). Consequently, the long-term morphological changes of these water systems are mainly associated with their tidal dynamics (Aubrey and Speers, 1985).

Various factors contribute to tidal asymmetry, resulting from the interaction between the astronomical tide and nonlinearities generated inside the estuary, including bottom friction, river inflow, bathymetric changes, and the morphology of such systems (Dronkers, 1986; Godin, 1991; Oliveira et al., 2006). Bottom frictions play the main role in the dissipation of tidal energy and transformation of the wave energy from the principal tidal constituents to several frequencies. These sets of frequencies are known as shallow water components of the tide (Boon, 2013). The shallow water components of tide are mainly referred to as the multiplying of principle frequencies, such as M4 and M6, representing the constituents generated from the principle semi-diurnal tidal constituent M2 and known as overtides or higher harmonics. Furthermore, the shallow water effects lead to the nonlinear interaction between the principal tidal constituents as well as the overtides, which can generate constituents with various frequencies and are known as compound tides, resulting from two or more constituents such as MN4, MS4, and MK3 (Gallo and Vizon, 2005; Hoitink et al., 2003). River inflow has substantial effects on the tidal dynamics of estuarine systems. However, river discharge can increase the average water level and thus reduce the tidal amplitudes and retards the celerity of tidal propagation, that is, deforming the tidal waves (Godin, 1985; Guo et al., 2015). Moreover, the morphology of the tidal systems can have an impact on their tidal dynamics. The funneling shape estuaries with reducing cross-sections can be damping the tidal wave energy by reflection against boundaries. In contrast, tidal waves can be amplified when the effects of the convergent overcome the effect of frictions. Consequently, tidal wave propagation exhibits a difference between high and low water, and deformation in the tidal wave occurs (Prandle, 2003).

Basically, there are two methods to recognize tidal asymmetry (Guo et al., 2019). The first is the harmonic method, which requires the calculations of amplitudes and phases of the interacted tidal constituents. This method depends on the phase difference between the interacted constituents in order to determine the direction of the tidal asymmetry and the ratio of the amplitudes to quantify the magnitude of the asymmetry (Parker, 2007). The second is the statistical method, which calculates the tidal probability density function and is known as a tidal skewness (Nidzieko, 2010; Song et al., 2011).

Shatt Al-Arab river is formed by the confluence of Euphrates and Tigris rivers at Qurna city in the Basrah province in southern Iraq and discharges to the Arabian Gulf (Figure 1). Shatt Al-Arab river estuary (SARE) represents an international border between Iraq and Iran. SARE has high importance for Basrah province as well as for many cities on the Iranian side. In addition to using its water for various residents' activities, the river is considered to be a navigation channel for shipping, oil transportation, and fishing (Lafta, 2021a). Several ports are located on the two river sides, principally depending on the tidal status in their overall activities (Abdullah et al., 2016; Al-Taei et al., 2014).

Tides of SARE follow the tidal regime of the Arabian Gulf. However, there are limited studies that highlighted the tidal dynamics of SARE. Generally, due to several reasons, the field measurements of physical characteristics in this estuary are scarce (Abdullah et al., 2015). The study of Al-Ramadhan and Pastour (1987) was the first study discussing the water movement in SARE. They indicated that the water dynamics in the estuary is governed by tidal effect and freshwater inflow. The tidal wave in SARE was analyzed by Abdullah (2002). The analysis was based on the data of 29 days of water level taken from the admiralty tide tables at the primary port of Iraq, known as an Outer Bar station. This station is located at the northwest tip of the Arabian Gulf, south of the SARE mouth (Figure 1). He illustrated that M2 constituent was the major tidal component. Moreover, he demonstrated that the tide displays a mixed, predominant semi-diurnal nature with the form number at 0.85. Abdullah (2014), based on the predicted water level acquired from the website (<http://easytide>), studied the characteristics of tidal phenomena in SARE. He demonstrated that the tidal wave undergoes attenuation as it propagates towards the upper reaches of the river, and the ebb duration was longer than the flood duration. Correspondingly, the aim of the current study is to examine the tidal dynamics and tidal wave deformation based on the continuous field measurements of water level at several locations along the estuary. However, according to our knowledge, there are no studies that explored the tidal dynamics in this estuary through the use of comprehensive field measurements of water level. In particular, to give a picture of tidal dynamics along SARE, evolution of tidal constituents and tidal deformation are discussed.

2. Material and methods

2.1. Study area

SARE is located in southern Iraq and represents the main source of freshwater discharging to the Arabian Gulf (Al-Yamani et al., 2020). The length of the river is about 200 km from Qurna city until it meets the Arabian Gulf at about 12 km south of Faw city (Figure 1). The river width exhibited a funnel shape nature. The width ranges from about 1000 m at its mouth and is reduced to 200 m at the Qurna. The bathymetry of the river is irregular, with the maximum and minimum depths reaching 18 and 6 m, respectively (Lafta, 2021a). Many islands formed along the river course as a result of river depositions, as well as tectonic and anthropogenic activities (Al-Whaely, 2014).

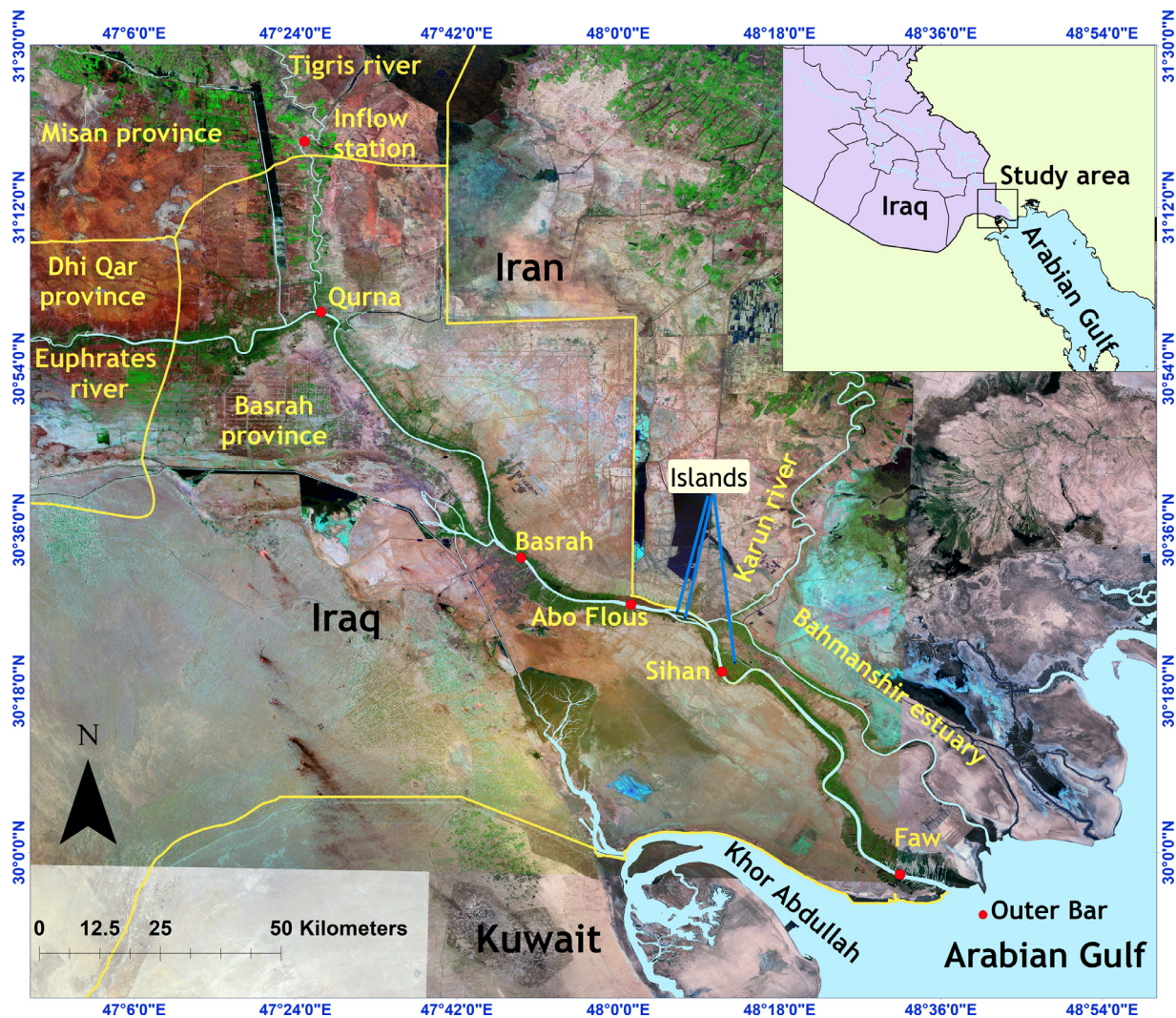


Figure 1 Location map of the study area showing the measurement locations of water level.

The hydrology of SARE is governed by the freshwater discharged from Tigris, Euphrates, and Karun rivers, the tidal force of the gulf, and the climatic conditions (Allafta and Opp, 2020). However, the continuous developments in the upstream countries of the Tigris, Euphrates, and Karun rivers result in very large reductions in the amounts of freshwater arriving at SARE. Additionally, the water resources authorities in Iraq exacerbate the problem after 2009, when the Euphrates river inflow towards SARE is completely segregated by constructing an embankment on its stream, about 35 km west of the Qurna site. Nowadays, due to these developments, SARE receives freshwater mainly from the Tigris river and minorly from the Karun river. These changes result in a pronounced alteration in the river hydrology and consequently affect the tidal propagation along the estuary.

2.2. Data collection

Water level measurements represent the main data required to conduct the study objective. However, the hourly water level records at four sites are conducted by installing water

level divers at Faw, Sihan, Abo Flous, and Basrah. The coordinates, distance to the estuary mouth, and length of the data record of these sites are given in Table 1.

The field measurements of water level were accomplished as cooperation between Marine Science Center/University of Basrah and Delft University of Technology during 2014. SARE is a high dynamics, and its navigation channel is always crowded by ships and fishermen's boats. Hence, all water level divers were installed inside steel pipes on the western bank of the estuary to overcome the undesired movement. These pipes contain several holes along their entire course to allow the water to flow through them.

Before installing these instruments, a controlling point on the land was determined by transferring its level relative to the local datum in this region, which is the mean sea level at Faw city (known as Faw 1979 datum). The differential global position system was utilized for transferring the level to the control points. Then, the divers were installed at suitable depths by taking into account that they are submerged during low and high tides.

Table 1 The coordinates, distance to the estuary mouth, and period of the data record at study stations.

Station	Longitude	Latitude	Distance to Estuary Mouth (km)	Period of Record
Faw	48°29.986'E	29°58.104'N	12	1/22/2014 to 1/9/2015
Sihan	48°11.973'E	30°19.423'N	67.7	1/25/2014 to 12/23/2014
Abo Flous	48°1.528'E	30°27.585'N	98.4	1/25/2014 to 12/23/2014
Basrah	47°50.098'E	30°32.041'N	119	3/26/2014 to 12/24/2014

2.3. Methodology

2.3.1. Harmonic analysis of tide

The harmonic method is widely utilized for investigating the tidal dynamics and tidal asymmetry in coastal systems (Iglesias et al., 2019; Lafta et al., 2020, 2021b; Mao et al., 2004; Siddig et al., 2019; Suh et al., 2014). This method is based on calculating the amplitudes and phases of the tidal constituents from the measured tidal data series (Boon, 2013).

The equation for the harmonic model is given as follows (Boon, 2013):

$$h(x, t) = h_0 + \sum_{j=1}^m f_j H_j \cos(\omega_j t + u_j - \kappa_j^*), \quad (1)$$

where t is the time in hours, $h(x, t)$ is the predicted water level, f_j is the lunar node factor for constituent, H_j is the amplitude for constituent, h_0 is the mean water level in that location, u_j is the nodal phase for constituent, κ_j^* is the phase of constituent, ω_j is the frequency of constituent, and m is the number of constituents. For purely solar constituents, $f_j = 1$ and $u_j = 0$. The Matlab worldtides, a package for tidal analysis, was used in this study. More details on this method, acquiring, and the application of this package can be found on the website (<https://www.mathworks.com/matlabcentral/fileexchange/24217-world-tides>).

However, tidal asymmetry can be generated when the interacted constituents satisfy $2\omega_1 = \omega_2$ and $\omega_1 + \omega_2 = \omega_3$ (ω is the constituent frequency) (Song et al., 2011). The relative phase relations, likely $2\theta_1 - \theta_2$ and $\theta_1 + \theta_2 - \theta_3$ (θ is the constituent phase in degrees), are mainly utilized for recognizing the nature of tidal deformation. In a semi-diurnal tidal system, for example, the interaction of the principal lunar semi-diurnal constituents M2 with its first harmonic M4 was broadly considered as the main cause that is responsible for tidal asymmetry (Aubrey and Speer, 1985; Friedrichs and Aubrey, 1988). The phase difference ($2\theta_1 = \theta_2$) in the range of 0 to 180 degrees refers to a shorter duration of the rising tide than the falling tide, or a flood dominance, while, in contrast, the phase difference in the range of 180 to 360 degrees refers to an ebb dominance tidal wave. When the phase difference was exactly 0 or 180 degrees, no tidal asymmetry will occur. Similarly, triad constituents interactions can lead to a tidal asymmetry. However, Song et al. (2011) examined the tidal wave deformation in 335 sea-level stations around the world. He reported that, in the mixed, mainly semi-diurnal tidal systems, the most significant triad interactions that can contribute to the total tidal asymmetry are M2-M4, M2-S2-MS4, M2-N2-MN4, M2-K1-O1, M2-K1-MK3, and M2-M4-M6. Similarly, the relative phase difference of these triad interactions in the

range of 0 to 180 degrees refers to a longer falling tide than the rising tide, thus flood dominance. Meanwhile, the phase differences in the range of 180 to 360 degrees refer to an ebb dominance tidal system (Song et al., 2011).

2.3.2. Tidal skewness

Tidal skewness is a statistical approach based on the calculation of the probability density function of water level proposed by Nidzieko (2010) and extended by Song et al. (2011). In this method, asymmetry from several constituents combinations taken into account, with only two or three combinations, could contribute to tidal skewness (Zhang et al., 2018). The most remarkable feature of this method is that it can determine the strength and relative contribution of each of such combinations into total tidal asymmetry based on the amplitudes, phases, and frequencies of the tidal constituents. The tidal skewness resulting from the combination of two tidal constituents is given as follows (Song et al., 2011):

$$\gamma_2 = \frac{\frac{3}{4} a_1^2 \omega_1^2 a_2 \omega_2 \sin(2\varphi_1 - \varphi_2)}{\left[\frac{1}{2} (a_1^2 \omega_1^2 + a_2^2 \omega_2^2) \right]^{\frac{3}{2}}}. \quad (2)$$

Meanwhile, the skewness resulting from the combinations of three constituents is given as follows (Song et al., 2011):

$$\gamma_3 = \frac{\frac{3}{2} a_1 \omega_1 a_2 \omega_2 a_3 \omega_3 \sin(\varphi_1 + \varphi_2 - \varphi_3)}{\left[\frac{1}{2} (a_1^2 \omega_1^2 + a_2^2 \omega_2^2 + a_3^2 \omega_3^2) \right]^{\frac{3}{2}}}, \quad (3)$$

where a_n , φ_n , and ω_n are amplitude, phase, and frequency of the tidal constituent. The contribution of the different combination to the overall tidal asymmetry is obtained as follows: for the combination of two constituents:

$$\beta_2 = \gamma_2 \left(\frac{a_1^2 \omega_1^2 + a_2^2 \omega_2^2}{\sum_{i=1}^N a_i^2 \omega_i^2} \right)^{\frac{3}{2}} \quad (4)$$

and for the combinations of three constituents:

$$\beta_3 = \gamma_3 \left(\frac{a_1^2 \omega_1^2 + a_2^2 \omega_2^2 + a_3^2 \omega_3^2}{\sum_{i=1}^N a_i^2 \omega_i^2} \right)^{\frac{3}{2}}. \quad (5)$$

Hence, the total skewness can be obtained by the summation of individual β :

$$\gamma_N = \sum \beta_2 + \sum \beta_3. \quad (6)$$

The direction of the tidal asymmetry is determined by the sign of the total skewness γ_N . The positive values of γ_N refer to a short period of rising water and long period of falling water, that is, the flood dominance, while the negative values of γ_N indicate the ebb dominance nature of tidal asymmetry.

2.3.3. Relative Sensitivity Coefficient (RSC)

The sensitivity of tidal asymmetry contributed by different combinations to the evolution of the amplitudes of tidal constituents can be examined by a nondimensional parameter known as a relative sensitivity coefficient (RSC) (Zhang et al. 2018).

The expression of RSC takes the form of two or three combinations (Yu et al. 2020): for the combination of two tidal constituents:

$$S_{a_1} = \frac{2a_2^2\omega_2^2 - a_1^2\omega_1^2}{a_1^2\omega_1^2 + a_2^2\omega_2^2}, \quad (7)$$

$$S_{a_2} = \frac{a_1^2\omega_1^2 - 2a_2^2\omega_2^2}{a_1^2\omega_1^2 + a_2^2\omega_2^2}, \quad (8)$$

and for the combination of three tidal constituents:

$$S_{a_1} = \frac{a_2^2\omega_2^2 + a_3^2\omega_3^2 - 2a_1^2\omega_1^2}{a_1^2\omega_1^2 + a_2^2\omega_2^2 + a_3^2\omega_3^2}, \quad (9)$$

$$S_{a_2} = \frac{a_1^2\omega_1^2 + a_3^2\omega_3^2 - 2a_2^2\omega_2^2}{a_1^2\omega_1^2 + a_2^2\omega_2^2 + a_3^2\omega_3^2}, \quad (10)$$

$$S_{a_3} = \frac{a_1^2\omega_1^2 + a_2^2\omega_2^2 - 2a_3^2\omega_3^2}{a_1^2\omega_1^2 + a_2^2\omega_2^2 + a_3^2\omega_3^2}, \quad (11)$$

where a and ω represents the amplitude and frequency of the tidal constituent, respectively. The RSCs values refer to the correlation between tidal skewness and constituent amplitude. However, the positive RSC implies the positive relationship between the tidal skewness and the amplitude; that is, tidal asymmetry will improve with the increase of the amplitude. In contrast, negative RSC suggests that tidal asymmetry will be reduced as the amplitude increases.

3. Results and discussion

3.1. Tidal harmonics

The time series measurements of water level are shown in Figure 2, which exhibits the spatial and spring-neap variability of the tidal range. The maximum tidal range was observed in the Faw station, reaching about 3 and 2.5 m in spring and neap tides, respectively. These ranges are nearly similar to the ranges recorded in estuary mouth by Shahidi et al. (2011), which are about 3.2 and 2.65 m in spring and neap tides, respectively. Meanwhile, the tidal range is highly reduced in Basrah station and reaches 0.5 m in spring tide. However, the reduction in the tidal ranges along the SARE reflect the continuous attenuation of the tidal wave when propagating further upstream.

The along-estuary variations in the amplitudes and phases of the tidal constituents (O1, K1, N2, M2, S2, MK3, MN4, M4, MS4, and M6) at the four locations are shown in Table 2. These ten tidal components explain over 92% of the total variance in water level at Faw station. Harmonic analysis results suggested that the tidal form numbers (O1+K1/M2+S2) range between 0.68 and 0.7. Hence, SARE is characterized by mixed, predominantly semi-diurnal tides according to the classification of Defant (Defant, 1960). This result is in accordance with the previous finding of Abdullah (2002). Among the main tidal constituents used in

the analysis, the largest was M2 in all stations. The second important constituent was K1, followed by O1, S2, and N2. The maximum amplitudes of the principal tidal constituents (M2, S2, N2, K1, and O1) were observed in the Faw station. However, it is obvious from Table 2 that the amplitudes of the semi-diurnal and diurnal tidal constituents have undergone a large reduction with distance along the longitudinal path of the estuary. The reduction in the constituents' amplitudes could be attributed to local bathymetry, that is, friction effect, which appears to exceed the effect of convergence nature of the estuary. As mentioned before, SARE is characterized by irregular depths along its course as well as the existence of several islands, particularly in the region located north and south of the confluence point of Karun river with SARE, as indicated in Figure 1. These islands can work as barriers that participate in the attenuation and nonlinear transformation of tidal energy and consequently the decay of the tidal harmonics. As illustrated by the results of the harmonic analysis (Table 2), most of the tidal energy is mainly dissipated near these islands, and this is reflected by the sharp decline of the amplitudes of the astronomical tidal constituents at Abo Flous station. However, Wu et al. (2018) demonstrated that the islands have a major effect on tidal hydrodynamics in tidal channels and make the tides more nonlinear. The reduction in the amplitudes of the tidal components towards inland direction was observed in many tidal systems, that is, Murray coastal lagoon (Jewell et al., 2012), Cochin estuary (Vinita et al., 2015), and Yangtze estuary (Lu et al., 2015).

The shallow water tidal constituents are generated when the tidal wave is distorted inside the estuary. The highest amplitudes of these constituents were observed near the estuary mouth (Faw station), except for M6. Unlike the M4 constituent, which is the most significant shallow water component in semi-diurnal tidal systems, MK3 was the largest shallow water constituent in the SARE. This could be because SARE is a mixed, mainly semi-diurnal tidal system, and the dominant astronomical components M2 and K1 control the tidal behavior. Consequently, the nonlinear transfer of energy from these two constituents gives a rise to MK3 among the other shallow water components. The second-largest shallow water constituent was M4, followed by MS4. These two constituents vary almost similarly due to their close frequencies. However, the evolution trend of the shallow water constituents displays a continuous reduction towards the inland direction, generally like the evolution of the principal astronomical components, except for the M6 and MK3. The M6 amplitude reaches its peak value at the Sihan station, about 61% relative to its amplitude at Faw station, and then decreases towards upper stations. In addition, the amplitude of the MK3 constituent showed a little increase between Abo Flous and Basrah stations, in comparison with its continuous reduction from Faw to Abo Flous stations. This inconsistent behavior of the shallow water components reflected the influences of the local geometry of the estuary in such regions.

The phase lags of all tidal constituents exhibited a gradual increase along the SARE. The tidal period in the SARE is close to the period of the M2 constituent, that is, 12.42 hours (Abdullah et al., 2016). Hence, the time of high and low water along the estuary is associated with the time of crest and trough of the M2 wave. However, according to

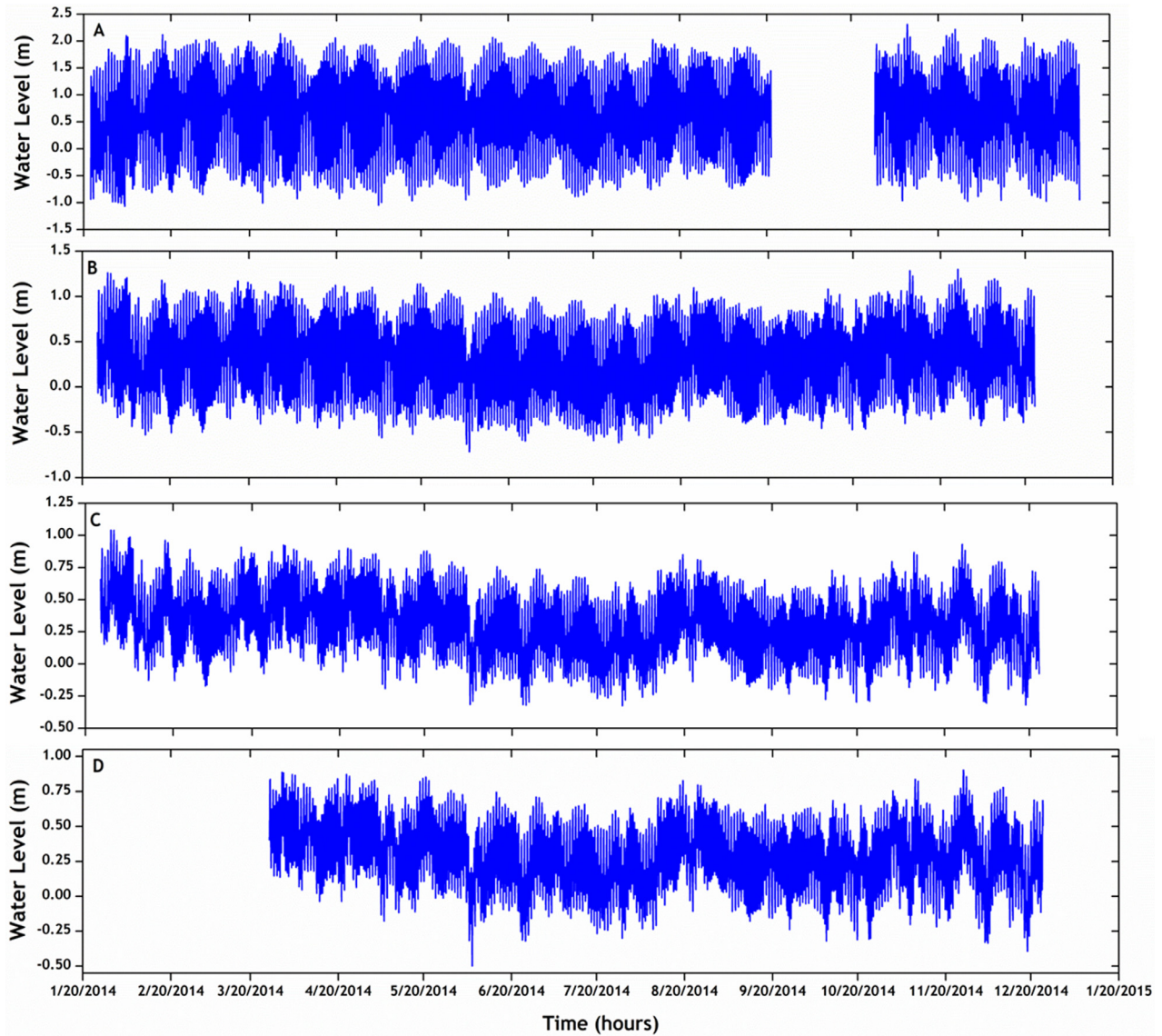


Figure 2 Time series of hourly water level records along the Shatt Al-Arab river estuary at Faw (A), Sihan (B), Abo Flous (c), and Basrah (D) stations during 2014.

Table 2 Amplitudes (m) and phases (degrees) for the tidal constituents used in the analysis.

Tidal Constituent	Faw		Sihan		Abo Flous		Basrah	
	Amp.	Phase	Amp.	Phase	Amp.	Phase	Amp.	Phase
O1	0.261	218.89	0.122	260.66	0.068	297.30	0.059	304.81
K1	0.449	305.53	0.277	346.40	0.133	22.59	0.129	32.58
N2	0.159	166.29	0.081	225.60	0.04	268.27	0.036	298.01
M2	0.799	278.58	0.443	342.32	0.23	28.39	0.221	54.09
S2	0.249	36.59	0.125	101.17	0.06	153.01	0.053	177.94
MK3	0.07	141.26	0.041	239.61	0.027	308.47	0.028	341.25
M4	0.049	110.10	0.03	261.64	0.015	350.85	0.014	30.99
MS4	0.039	236.95	0.022	22.15	0.011	109.57	0.008	154.10
MN4	0.017	2.17	0.009	156.61	0.005	256.09	0.004	299.08
M6	0.005	223.8	0.013	79.98	0.011	202.85	0.008	265.33

Hicks (2006) and Kuang et al. (2017), the time corresponding to the phase lag of the tidal constituent can be estimated by the following:

$$Time = \frac{\Delta G}{360} \times T_{cont.}$$

where ΔG is the phase lag between two locations and $T_{cont.}$ is the period of the tidal constituent. The results revealed that the phase lags of the semi-diurnal constituents increase faster than the phase lags of the diurnal constituents. This is mainly related to the effect of friction, which is proportional to the square of the wave speed (Parker, 2007); that is, wave speeds of semi-diurnal constituents are slower than those diurnal constituents. However, according to Hicks (2006), the speed of the tidal constituents is $360^\circ/T_{cont.}$; hence, semi-diurnal constituents decay faster than the diurnal constituents under the effects of friction. This result is consistent with the theoretical indication of Godin (1999), which illustrated that the decay rate of the tidal constituents is frequency-dependent; that is, constituents with higher frequencies decay faster. The phase lag of M2 ($T_{M2} = 12.42$ hours) between Faw and Sihan stations reaches 63.74 degrees; that is, high water, or wave crest, takes about 2.19 hours between these two stations. By taking into account that the distance between Faw and Sihan stations reaches 55 km, hence tidal wave propagates with speed at about 25 km/h. As the tidal wave moves further upstream, a pronounced delay in speed occurs. The phase lag of M2 reaches 46.07 degrees between Sihan and Abo Flous stations, and hence, high water needs about 1.58 hours to cover the distance between these two locations. The distance between Sihan and Abo Flous is about 31 km, and consequently, the tidal wave propagates at a speed that reaches 21 km/hour. The phase lag reaches 135.51 degrees between Faw and Basrah station; that is, about 4.67 hours are required for the tidal wave to move from Faw to Basrah station. The phase lags of the S2 and N2 exhibited a similar evolution trend as M2 but with a few different magnitudes as a result of their different periods. Additionally, the phase lags of the diurnal constituents also showed gradual increases towards upstream. For instance, the phase lag of K1 between Faw and Basrah stations reaches 87.05 degrees. Based on the period of the K1, which equals 23.93 hours, the time required by this wave to move from Faw to Basrah station reaches 5.78 hours. However, since the wave speed of K1 is about half of the speed of M2 (Hicks, 2006), and by comparison of the time required by M2 and K1 to move from Faw to Basrah stations, it is obvious that semi-diurnal constituents experience a large delay along the estuary. Meanwhile, the phase lags for the shallow water constituents are related to their frequencies and increase faster than the astronomical constituents towards upstream under the effect of nonlinear friction.

3.2. Tidal asymmetry

Tidal asymmetry can be created by the combinations of two or more constituents, both astronomical or mixed between astronomical and shallow water constituents (Guo et al., 2019; Provost, 1991; Song et al., 2011).

The results of the harmonic method indicated that the relative phase relation between M2 and M4 ($2\theta_{M2} - \theta_{M4}$)

at the Faw station is 87.06 degrees and varies along the estuary with 63, 65.93, and 77.19 degrees in Sihan, Abo Flous, and Basrah stations, respectively. Hence, according to Aubrey and Speer (1985), SARE exhibits a flood dominance behavior if only the M2-M4 interaction is taken into account. According to Lu et al. (2015), the M4/M2 amplitude ratio that is greater than 0.01 indicates the significant tidal distortion in the tidal system. In SARE, this ratio ranged between 0.061 and 0.067 and exhibited an inconsistent evolution trend by increasing from Faw towards Sihan, and then, it displayed a little reduction towards the other stations. However, the evolution of this ratio depends on the behavior of both M2 and M4. The spatial distribution of this ratio is highly dependent on the local geometry of the estuary, and when it increases, it refers to the large transfer of energy from M2 to M4.

Tidal asymmetry was investigated further by the tidal skewness metrics. Following Song et al. (2011), the tidal asymmetry in SARE can be induced by several interactions, such as M2-M4, M2-K1-O1, M2-S2-MS4, M2-K1-MK3, M2-N2-MN4, and M2-M4-M6. However, the relative phase relations for all these interactions ranged between 5 and 179 degrees, suggesting a flood dominance tidal asymmetry in the estuary. These results are mainly consistent with the observed longer period of the ebb tide than the flood tide and are in agreement with the previous indications of Abdullah (2014). Figure 3 displays the mean values of the tidal skewness at all stations. Positive values of tidal skewness were observed at all stations, indicating a longer period of the falling tide than the rising tide. The steadily increasing tidal skewness reflected the continuous tidal wave deformation towards the upper reaches of the estuary.

The highest values of tidal skewness were recorded at Basrah and Sihan stations, indicating the nonuniform behavior of tidal wave deformation along the SARE. However, increasing the tidal skewness at the middle reaches of the estuary, that is, at Sihan station, could be mainly attributed to the local characteristics of the estuary as well as to the freshwater inputs from the Karun river, which is sufficient to prolong the ebb duration, and consequently more tidal deformation at this region will occur. Similar behavior of nonuniform tidal wave deformations was observed in several estuaries in the world, that is, the upper St. Lawrence (Godin 1985, 1999), the Amazon estuary (Gallo and Vizon, 2005), and Changjiang river estuary (Guo et al., 2019). Furthermore, Figure 3 illustrates the contributions of the six combinations to total tidal skewness. The nonlinear interaction between M2 and its first harmonic M4 appears to be the dominant contributor to tidal asymmetry, with a gradual evolution along the estuary. This interaction accounts for 49.17, 51.73, 54.67, and 54.45% of the total skewness at Faw, Sihan, Abo Flous, and Basrah stations, respectively. However, asymmetry generated by this interaction is traditionally increased by the reduction of M2 amplitude and generation of M4, and obviously, this is the case at SARE, which displayed a large reduction of the M2 amplitude towards inland stations. Such behavior was commonly recorded in many estuaries around the world, like the Amazon estuary (Gallo and Vizon, 2005), Yangtze estuary (Lu et al., 2015), and Pearl river delta (Zhang et al., 2018). The interaction of the astronomical M2-K1-O1 triad represents the second main contributor to the tidal asymmetry,

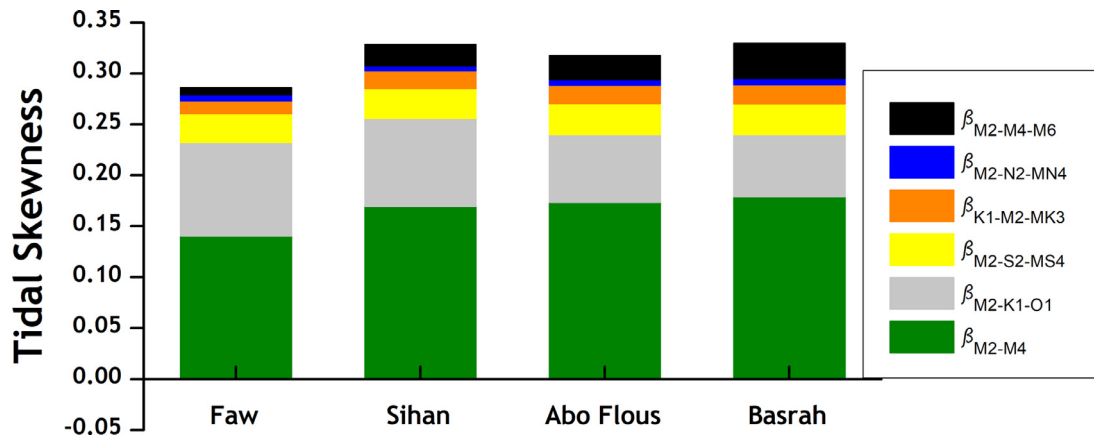


Figure 3 The contributions of the six combinations to total tidal skewness along the Shatt Al-Arab river estuary.

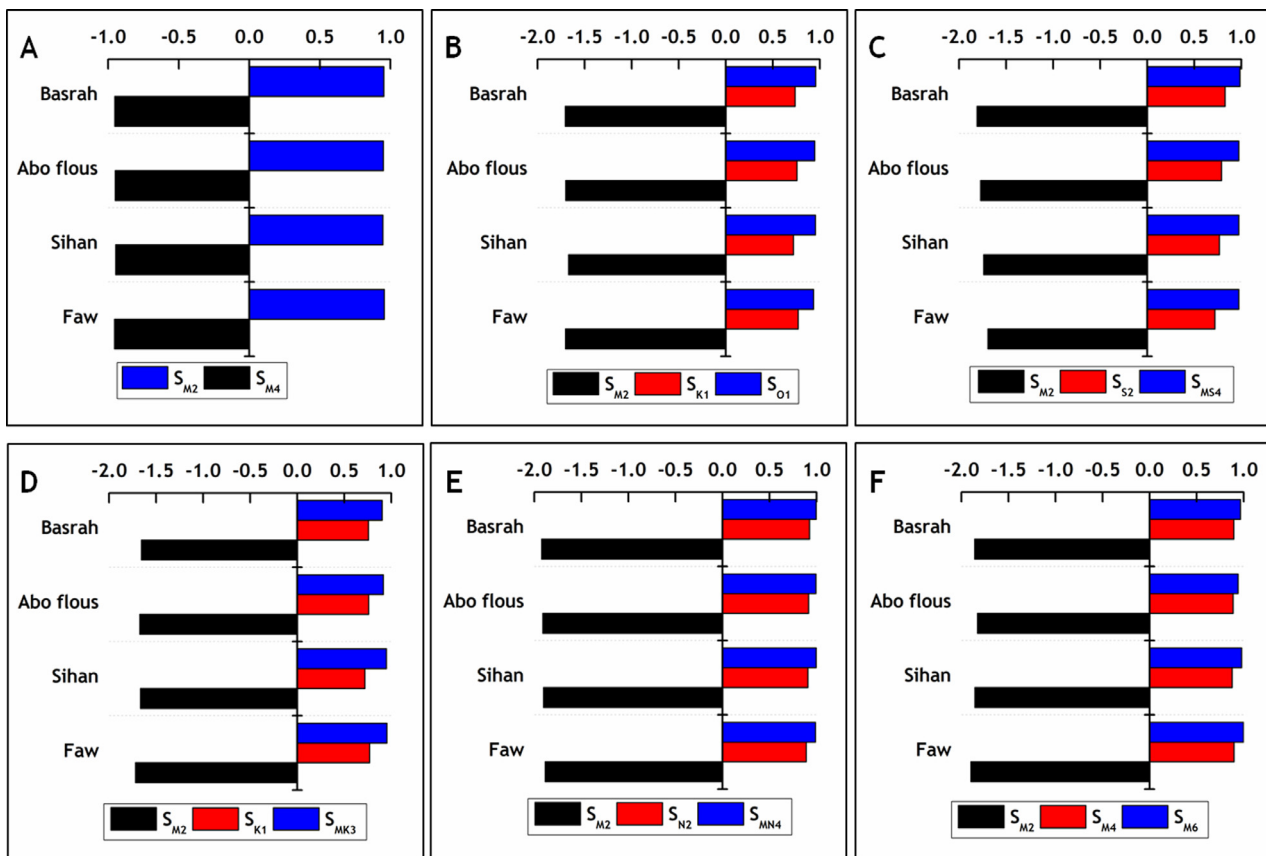


Figure 4 The mean value of relative sensitivity coefficient for different constituents amplitudes contributing to total tidal skewness by M2-M4 (A), M2-K1-O1 (B), M2-S2-MS4 (C), M2-K1-MK3 (D), M2-N2-MN4 (E), and M2-M4-M6 (F) along the Shatt Al-Arab river estuary.

accounting for 32.18, 26.26, 21.03, and 18.42% at four stations, respectively. However, although a substantial decline in the skewness of this interaction occurs towards the inland direction, due to the large reduction of the amplitudes of astronomical constituents, the tidal asymmetry induced by this triad combination is a flood dominant in SARE. This indicates that the tide is mostly a flood dominant in offshore before entering the estuary. It is well known that the northern Arabian Gulf is a shallow water region with maximum

depths that do not exceed 20 m (Lafta et al., 2019). Hence, the nonlinear friction in shallow water plays a fundamental role in tidal wave deformation in the northern part of the gulf, resulting in the retard of the tidal wave propagation around low tides to high tides. Similar behaviors of the M2-K1-O1 interaction were observed in some estuarine systems, such as the Cochin estuary (Vinita et al., 2015) and Yangtze estuary (Yu et al., 2020). The M2-S2-MS4 interaction seems to be the third contributor, participating by about

9–10% to the total skewness. The considerable attenuation of both M2 and S2 constituents inside the estuary gave rise to this interaction. However, Song et al. (2011) indicated that, in mixed semi-diurnal tidal systems, M2-S2-MS4 interaction plays a fundamental role in the tidal asymmetry in such systems. The fourth important interaction was M2-M4-M6 with contribution percentage rising from 2% at Faw to 10% at Basrah station. This rise was expected as the M2 constituent experiences more reduction in the upper reaches of the estuary. The interaction of K1-M2-MK3 seems to have a secondary effect on the tidal asymmetry at all stations, with the largest contribution reaching about 5% at Basrah station. While the M2-N2-MN4 interaction has a minor role in the total asymmetry with the contribution not exceeding 2%, this can be attributed to the small amplitudes for both N2 and MN4 constituents.

3.3. Influence of tidal evolution on tidal asymmetry

Sensitivity analysis is conducted to quantify the response of the tidal skewness to the evolution of the tidal constituents along SARE. Figure 4 illustrates the relative sensitivity coefficients for the six combinations contributing to the tidal asymmetry in SARE. The results revealed that RSC for M2 amplitude is negative for all six combinations. This implies that the tidal asymmetry is enhanced by a reduction in the M2 amplitude. The tidal asymmetry induced by the M2-M4 combination is mainly intensified by increasing M4 amplitude and decreasing the M2 amplitude. However, our results showed a relative reduction in the M4 amplitude, which is expected to minimize the tidal skewness of M2-M4 along the estuary. In contrast, a substantial increase in tidal skewness of M2-M4 was observed towards the upper reaches of estuary. This behavior is mainly due to the large reduction in the M2 amplitude in comparison with M4 amplitude along the estuary. Regarding tidal skewness induced by the M2-K1-O1 combination, the relative sensitivity coefficient implies that tidal asymmetry is enhanced by increasing K1 and O1 amplitudes and decreasing the M2 amplitude. The results indicated that tidal skewness that resulted from M2-K1-O1 asymmetry experienced a significant reduction towards the upper reaches of the estuary, despite the substantial attenuation of M2 amplitude. However, both K1 and O1 amplitudes showed a large reduction as they propagate towards the inland direction, leading to an obvious minimizing of the M2-K1-O1 asymmetry. The sensitivity coefficient of M2 for the M2-M4-M6 combination is also negative. The tidal asymmetry induced by this combination undergoes a significant increase towards the inland areas and is associated with a large reduction that occurs in the M2 amplitude, in the same way as the M2-M4 combination. The sensitivity coefficients of M2 for the remaining combinations, including M2-S2-MS4, M2-K1-MK3, and M2-N2-MN4, are also negative. However, all these three combinations illustrated a relative increase along the estuary due to the reduction that occurs in M2 amplitude. Consequently, the reduction of M2 amplitude plays a fundamental role in intensifying the tidal asymmetry in SARE.

4. Conclusions

In this study, the water level measurements indicated that the tidal wave experiences pronounced damping when propagating towards the inland direction. Consequently, the friction effect was overcoming the convergent nature of the estuary. The maximum tidal ranges at the seaside station were 3 and 2.5 m in spring and neap tides, respectively, and decreased in the upper reaches of the estuary. The results of the harmonic analysis indicated that the amplitudes of the principles diurnal K1 and O1 and semi-diurnal M2 and S2 experience considerable reductions towards the inland direction under the effect of friction and the geometry of the estuary. Hence, in this context, higher and compound tides were generated.

Six possible interactions, including the astronomical and nonlinearities to the total asymmetry, were evaluated. The main contributor to the tidal wave deformation coincides with the interaction of M2 and M4 at all stations, followed by other interactions. The results of both the harmonic method and the tidal skewness method demonstrated that SARE exhibited a flood dominance nature of tidal asymmetry. The nonuniform behavior of tidal asymmetry was recognized. The Basrah and Sihan stations presented a more tidal wave deformation due to the local characteristics as well as the effect of the freshwater inflow. The relative sensitivity coefficient of M2 appears to have the largest values in all combinations; hence, the tidal asymmetry of SARE is mainly sensitive to variations in the M2 amplitude.

It is worth mentioning that the results obtained are mainly based on the water level measurements and focused on the tidal duration asymmetry due to the lack of flow velocity data. Hence, it is highly recommended to investigate the velocity asymmetry that is directly correlated with the sediment dynamics and morphological evolution in coastal systems. Additionally, it is highly recommended to study the influence of the river discharge variations on the tidal dynamics. This could be conducted based on the numerical modeling techniques.

Acknowledgments

The author is grateful to the technician team of the Marine Science Center/ University of Basrah for their helping in the field works.

References

- Abdullah, S.S., Lafta, A.A., Al-Taei, S.A., Al-Kaabi, A.H., 2016. Flushing Time of Shatt Al-Arab River. South of Iraq. *Mesopot. J. Mar. Sci.* 31 (1), 61–74.
- Abdullah, A.D., Masih, I., van der Zaag, P., Karim, U.F.A., Popescu, I., Al Suhail, Q., 2015. Shatt al Arab River system under escalating pressure: a preliminary exploration of the issues and options for mitigation. *Int. J. River Basin Manage.* 13 (2), 215–227. <https://doi.org/10.1080/15715124.2015.1007870>
- Abdullah, S.S., 2002. Analysis of Tide Wave in Shatt Al-Arab Estuary, South of Iraq. *Mesopot. J. Mar. Sci.* 17 (2), 305–315.
- Abdullah, S.S., 2014. Tide phenomena in the Shatt Al-Arab River, South of Iraq. *Journal of the Arabian Gulf* 42 (3), 133–155.

- Allafta, H., Opp, C., 2020. Spatio-temporal variability and pollution sources identification of the surface sediments of Shatt Al-Arab River. Southern Iraq. *Scient. Rep.* 10 (6979), 1–16. <https://doi.org/10.1038/s41598-020-63893-w>
- Al-Ramadhan, B.M., Pastour, M., 1987. Tidal characteristics of Shatt Al-Arab River. *Mesopot. J. Mar. Sci.* 2 (1), 15–28.
- Al-Taei, S.A., Abdullah, S.S., Lafta, A.A., 2014. Longitudinal intrusion pattern of salinity in Shatt Al Arab estuary and reasons. *J. KAU: Mar. Sci.* 25 (2), 205–221. <https://doi.org/10.4197/Mar.25-2.10>
- Al-Whaely, U.Q., 2014. Origin and evolution of the Islands of the Shatt Al-Arab River southern Iraq. Ph.D. Thesis, College of Science, Univ. Basrah, 143 pp (in Arabic).
- Al-Yamani, F.Y., Polikarpov, I., Saburova, M., 2020. Marine life mortalities and harmful algal blooms in the Northern Arabian Gulf. *Aquat. Ecosyst. Health* 23, 196–209. <https://doi.org/10.1080/14634988.2012.679450>
- Aubrey, D.G., Speer, P.E., 1985. A study of non-linear tidal propagation in shallow inlet/estuarine systems. Pt. I: Observations. *Estuar. Coast. Shelf Sci.* 21 (2), 185–205. [https://doi.org/10.1016/0272-7714\(85\)90096-4](https://doi.org/10.1016/0272-7714(85)90096-4)
- Boon, J.D., 2013. *Secrets of the Tide: Tide and Tidal Current Analysis and Predictions, Storm Surges and Sea Level Trends.* Elsevier, 224.
- Defant, A., 1960. In: *Physical oceanography, 2.* Peragamon Press, Oxford, 598.
- Dronkers, J., 1986. Tidal asymmetry and estuarine morphology. *Netherlands J. Sea Res.* 20 (2), 107–131. [https://doi.org/10.1016/0077-7579\(86\)90036-0](https://doi.org/10.1016/0077-7579(86)90036-0)
- Friedrichs, C.T., Aubrey, D.G., 1988. Non-linear tidal distortion in shallow well-mixed estuaries: A synthesis. *Estuar. Coast. Shelf Sci.* 27 (5), 521–545. [https://doi.org/10.1016/0272-7714\(88\)90082-0](https://doi.org/10.1016/0272-7714(88)90082-0)
- Gallo, M.N., Vinzon, S.B., 2005. Generation of overtides and compound tides in the Amazon estuary. *Ocean Dynam.* 55 (5), 441–448. <https://doi.org/10.1007/s10236-005-0003-8>
- Gatto, V.M., van Prooijen, B.C., Wang, Z.B., 2017. Net sediment transport in tidal basins: quantifying the tidal barotropic mechanisms in a unified framework. *Ocean Dynam.* 67, 1385–1406. <https://doi.org/10.1007/s10236-017-1099-3>
- Godin, G., 1999. The propagation of tides up rivers with special considerations on the upper Saint Lawrence river. *Estuar. Coast. Shelf Sci.* 48, 307–324. <https://doi.org/10.1006/ecss.1998.0422>
- Godin, G., 1985. Modification of river tides by the discharge. *J. Water. Port Coast. Ocean Eng.* 111 (2), 257–274. [https://doi.org/10.1061/\(ASCE\)0733-950X\(1985\)111:2\(257\)](https://doi.org/10.1061/(ASCE)0733-950X(1985)111:2(257))
- Godin, G., 1991. Frictional effects in river tides. In: Parker, B.B. (Ed.), *Tidal Hydrodynamics.* John Wiley, Toronto, 379–402.
- Guo, L., Wang, Z.B., Townend, I., He, Q., 2019. Quantification of Tidal Asymmetry and Its Nonstationary Variations. *J. Geophys. Res.-Ocean.* 124 (1), 773–787. <https://doi.org/10.1029/2018JC014372>
- Guo, L.C., van der Wegen, M., Jay, D.A., Matte, P., Wang, Z.B., Roelvink, J.A., He, Q., 2015. River-tide dynamics: Exploration of nonstationary and nonlinear tidal behavior in the Yangtze River estuary. *J. Geophys. Res.-Oceans* 120, 3499–3521. <https://doi.org/10.1002/2014JC010491>
- Hicks, S.D., 2006. *Understanding Tides.* NOAA, National Ocean Service, 83 pp.
- Hoitink, A.J., Hoekstra, P., Van Maren, D.S., 2003. Flow asymmetry associated with astronomical tides: implications for the residual transport of sediment. *J. Geophys. Res.* 108 (C10), 3315. <https://doi.org/10.1029/2002JC001539>
- Iglesias, I., Ailez-Valente, P., Bio, A., Bastos, L., 2019. Modeling the main hydrodynamic pattern in shallow water estuaries: The Minho case study. *Water* 1 (5), 1040. <https://doi.org/10.3390/w11051040>
- Jewell, S.A., Walker, D.J., Fortunato, A.B., 2012. Tidal asymmetry in a coastal lagoon subject to a mixed tidal regime. *Geomorphology* 138 (1), 171–180. <https://doi.org/10.1016/j.geomorph.2011.08.032>
- Kuang, C., Liang, H., Mao, X., Karney, B., Gu, J., Huang, H., Chen, W., Song, H., 2017. Influence of potential future sea-level rise on tides in the China sea. *J. Coast. Res.* 33 (1), 105–117. <https://doi.org/10.2112/JCOASTRES-D-16-00057.1>
- Lafta, A.A., 2021a. Estimation of Tidal excursion Length Along The Shatt Al-Arab Estuary, Southern Iraq. *Vietnam J. Sci. Tech.* 59 (1). <https://doi.org/10.15625/2525-2518/59/1/15433>
- Lafta, A.A., 2021b. Influence of atmospheric forces on sea surface fluctuations in Iraq marine water, northwest of Arabian Gulf. *Arab. J. Geo.* 14, 1639. <https://doi.org/10.1007/s12517-021-07874-x>
- Lafta, A.A., Al-Taei, S.A., Al-Hashimi, N.H., 2019. Characteristics of the tidal wave in Khor Abdullah and Khor Al-Zubair Channels, Northwest of the Arabian Gulf. *Mesopot. J. Mar. Sci.* 34 (2), 112–125.
- Lafta, A.A., Altaei, S.A., Al-Hashimi, N.H., 2020. Impacts of potential sea-level rise on tidal dynamics in Khor Abdullah and Khor Al-Zubair, northwest of Arabian Gulf. *Earth Syst. Environ.* 4, 93–105. <https://doi.org/10.1007/s41748-020-00147-9>
- Lu, S., Tong, C., Lee, D.Y., Zheng, J., Shen, J., Zhang, W., Yan, Y., 2015. Propagation of tidal waves up in Yangtze Estuary during the dry season. *J. Geophys. Res.-Oceans* 120 (9), 6445–6473. <https://doi.org/10.1002/2014JC010414>
- Mao, Q., Shi, P., Yin, K., Gan, J., Qi, Y., 2004. Tides and tidal currents in the Pearl River Estuary. *Contin. Shelf Res.* 24, 1797–1808. <https://doi.org/10.1016/j.csr.2004.06.008>
- Nidziko, N.J., 2010. Tidal asymmetry in estuaries with mixed semidiurnal/diurnal tides. *J. Geophys. Res.* 115, C08006. <https://doi.org/10.1029/2009JC005864>
- Oliveira, A., Fortunato, A.B., Regob, J.R., 2006. Effect of morphological changes on the hydrodynamics and flushing properties of the Óbidos lagoon (Portugal). *Cont. Shelf Res.* 26 (8), 917–942. <https://doi.org/10.1016/j.csr.2006.02.011>
- Parker, B.B., 2007. *Tidal Analysis and Prediction.* National Ocean Service, NOAA Spec. Publ. <https://doi.org/10.25607/OBP-191>
- Prandle, D., 2003. Relationships between tidal dynamics and bathymetry in strongly convergent estuaries. *J. Phys. Oceanogr.* 33 (12), 2738–2750. [https://doi.org/10.1175/1520-0485\(2003\)033<2738:RBTDB>2.0.CO;2](https://doi.org/10.1175/1520-0485(2003)033<2738:RBTDB>2.0.CO;2)
- Provost, L.C., 1991. Generation of overtides and compound tides (review). In: Parker, B.B. (Ed.), *Tidal Hydrodynamics.* John Wiley, Toronto, 269–295.
- Pugh, D.T., 1987. *Tides, surges and mean sea-level.* John Wiley, New York, 486 pp.
- Shahidi, A.E., Parsa, J., Hajiani, M., 2011. Salinity intrusion length: comparison of different approaches. *Mar. Eng.* 164 (1), 33–43. <https://doi.org/10.1680/maen.2011.164.1.33>
- Siddig, N.A., Al-Subhi, A.M., Alsaafani, M.A., 2019. Tide and mean sea level trend in the west coast of the Arabian Gulf from tide gauges and multi-missions satellite altimeter. *Oceanologia* 61 (4), 401–411. <https://doi.org/10.1016/j.oceano.2019.05.003>
- Song, D., Wang, X.H., Kiss, A.E., Bao, X., 2011. The contribution to tidal asymmetry by different combinations of tidal constituents. *J. Geophys. Res.* 116, C12007. <https://doi.org/10.1029/2011JC007270>
- Suh, S.W., Lee, H.Y., Kim, H.J., 2014. Spatio-temporal variability of tidal asymmetry due to multiple coastal constructions along the west coast of Korea. *Estuar. Coast. Shelf Sci.* 151, 336–346. <https://doi.org/10.1016/j.ecss.2014.09.007>
- Vinita, J., Shivaprasad, A., Manoj, N.T., Revichandran, C., Naveenkumar, K.R., Jineesh, V.K., 2015. Spatial tidal asymmetry of Cochin estuary, West Coast, India. *J. Coast. Conserv.* 19, 537–551. <https://doi.org/10.1007/s11852-015-0405-9>

- Wu, R., Jiang, Z., Li, C., 2018. Revisiting the tidal dynamics in the complex Zhoushan Archipelago waters: a numerical experiment. *Ocean Model.* 132, 139–156. <https://doi.org/10.1016/j.ocemod.2018.10.001>
- Yu, X., Zhang, W., Hoitink, A.J.F., 2020. Impact of river discharge seasonality change on tidal duration asymmetry in the Yangtze river estuary. *Sci. Rep.* 10, 6304. <https://doi.org/10.1038/s41598-020-62432-x>
- Zhang, W., Cao, Y., Zhu, Y., Zheng, J., Ji, X., Xu, Y., Wu, Y., Hoitink, A.J.F., 2018. Unravelling the causes of tidal asymmetry in deltas. *J. Hydrol.* 564, 588–604. <https://doi.org/10.1016/j.jhydrol.2018.07.023>